TUDelft

Delft University of Technology

Kirkwood–Buff integrals of finite systems
Shape effects

Dawass, Noura; Krüger, Peter; Simon, Jean Marc; Vlugt, Thijs J.H.

Important note
To cite this publication, please use the final published version (if applicable).
Please check the document version above.

Taylor & Francis
Taylor & Francis Group

RESEARCH ARTICLE

Kirkwood–Buff integrals of finite systems: shape effects

Noura Dawass [a], Peter Krüger [b], Jean-Marc Simon [c] and Thijs J. H. Vlugt [a]

[a]Process & Energy Laboratory, Delft University of Technology, Delft, The Netherlands; [b]Graduate School of Science and Engineering, Chiba University, Chiba, Japan; [c]CNRS-Université de Bourgogne Franche-Comté, Dijon, France

ABSTRACT

The Kirkwood–Buff (KB) theory provides an important connection between microscopic density fluctuations in liquids and macroscopic properties. Recently, Krüger *et al.* derived equations for KB integrals for finite subvolumes embedded in a reservoir. Using molecular simulation of finite systems, KB integrals can be computed either from density fluctuations inside such subvolumes, or from integrals of radial distribution functions (RDFs). Here, based on the second approach, we establish a framework to compute KB integrals for subvolumes with arbitrary convex shapes. This requires a geometric function $w(x)$ which depends on the shape of the subvolume, and the relative position inside the subvolume. We present a numerical method to compute $w(x)$ based on Umbrella Sampling Monte Carlo (MC). We compute KB integrals of a liquid with a model RDF for subvolumes with different shapes. KB integrals approach the thermodynamic limit in the same way: for sufficiently large volumes, KB integrals are a linear function of area over volume, which is independent of the shape of the subvolume.
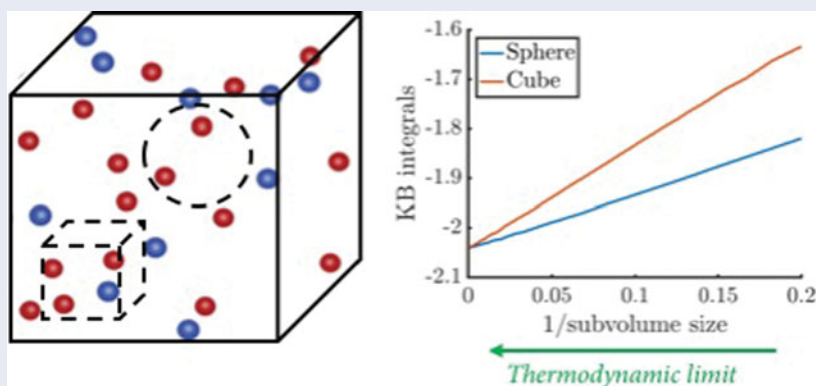
1. Introduction

Density and energy fluctuations inside subvolumes embedded in a larger reservoir can be used to determine macroscopic thermodynamic properties of multicomponent isotropic liquids [1–5]. Recently, Schnell *et al.* [2] derived the Small System Method (SSM) where fluctuations inside finite subvolumes are extrapolated to the thermodynamic limit. Using the SSM, thermodynamic properties like partial molar enthalpies and thermodynamic factors were calculated, and in the same manner, Kirkwood–Buff (KB) integrals were obtained [5–8]. The KB theory provides a sound connection between the microscopic structure of isotropic liquids and their macroscopic properties [9–13]. Kirkwood and Buff [9]

defined these integrals for infinitely large and open systems. To compute KB integrals using molecular simulations of closed and finite systems, Krüger *et al.* [14] recently derived expressions for KB integrals for open subvolumes embedded in a large reservoir. For multicomponent isotropic systems, these KB integrals for finite subvolumes, $G_{\alpha\beta}^V$, are related to the fluctuations of the number of molecules inside a finite and open subvolume,

$$G_{\alpha\beta}^V \equiv V \frac{\langle N_\alpha N_\beta \rangle - \langle N_\alpha \rangle \langle N_\beta \rangle}{\langle N_\alpha \rangle \langle N_\beta \rangle} - \frac{V \delta_{\alpha\beta}}{\langle N_\beta \rangle}, \quad (1)$$

where N_α, N_β are the number of molecules of types α and β inside the subvolume V (N_α and N_β fluctuate due
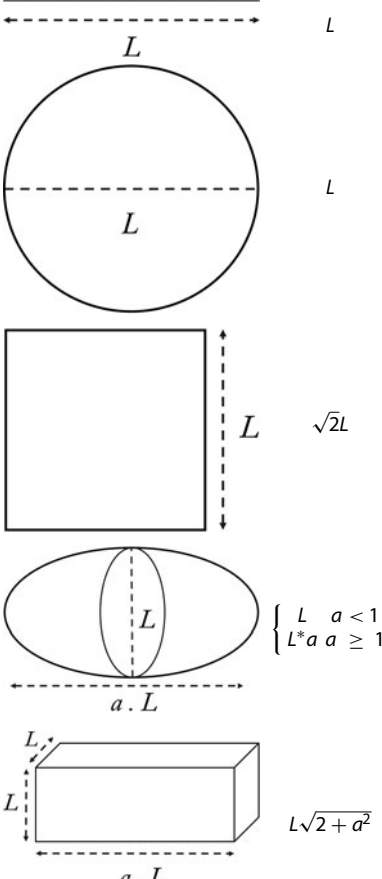
Table 1. Subvolume shapes considered in this work. L is the characteristic linear dimension of the shape and $L_{\max}$ is the largest possible distance between two points inside the subvolume. A cube and sphere are included as special cases of cuboid and spheroid with aspect ratio $a = 1$.

Shape of the subvolume		$L_{\max}$
Line (1D)		L
Circle (2D)		L
Square (2D)		$\sqrt{2}L$
Spheroid (3D)		$\begin{cases} L & a < 1 \\ L{*}a & a \geq 1 \end{cases}$
Cuboid (3D)		$L\sqrt{2 + a^2}$

Table 2. Exact expressions of the geometrical function $w(x)$ for hyperspheres in 1–3 dimensions (i.e. line, circle, and sphere) [14]. Here, $x = r/L_{\max}$ ($0 < x < 1$) and $c(r)\mathrm{d}r$ is the hyperspherical volume element.

Dimension	$c(r)$	$w(x)$
1D	2	$1 - x$
2D	$2\pi r$	$2/\pi \left(\arccos(x) - x\sqrt{1 - x^2}\right)$
3D	$4\pi r^2$	$1 - 3x/2 + x^3/2$

where $g_{\alpha\beta}(r)$ is the radial distribution function. $L_{\max}$ is the largest distance between two points inside the subvolume V (see Table 1). $c(r)\,\mathrm{d}r$ is the hyperspherical volume element (see Table 2). $w(x)$ is a geometrical function, which depends on the dimensionality and shape of the subvolume V, as well as on $x = r/L_{\max}$, where $r = |\mathbf{r}_1 - \mathbf{r}_2|$ is the pair distance. The integration limit $L_{\max}$ is therefore also present in the integrand. By construction, the definitions of $w(x)$ and $c(r)$ automatically lead to $w(0) = 1$ and $w(1) = 0$. For a hypersphere in D dimensions, $w(x)$ is known analytically [14]. The theoretical derivation of Equations (1) and (2) and the function $w(x)$ for a sphere is provided in our recent publication [4]. It is important to note that Equations (1) and (2) are identical and yield the same KB integral provided that the subvolume V is convex and the function $w(x)$ corresponding to the shape of V is used. Both approaches (Equation (1) and Equation (2)) have been used in molecular simulation [4–6,8,14–16]. The advantage of using Equation (2) is that only the RDF is needed, which is usually computed from a built-in function of Molecular Dynamics software [17].

Considering the shape of the subvolume, the sphere is the most natural choice in simple isotropic liquids, but other shapes may be more convenient for specific applications. For example, the KB theory was applied to study the interactions between large biomolecules and the surrounding solvent molecules [18–20]. Giambasu *et al.* [21] used KB integrals to study the ionic atmosphere surrounding nucleic acids. In their work, selecting the shape of the subvolume depended on the inhomogeneous region surrounding the nucleic acids [21]. For instance, hexagonal prisms were used to study the fluctuations of solvent molecules around DNA. In principle, it is possible to compute KB integrals using Equation (1) for any shape of the subvolume. The size of the subvolume can be gradually increased as shown in Figure 1, and the number of particles in each subvolume is then used to compute $G_{\alpha\beta}^V$ using Equation (1). Cubic subvolumes have been used in the works of Schnell *et al.* [1], Cortes-Huerto *et al.* [22] and others [15,17,23]. The alternative formulation of finite-size KB integrals (Equation (2)), i.e. direct integration of the RDF, has only been applied to spherical subvolumes [6,14]. It is important to note that

to molecule exchanges with the surrounding reservoir), and the brackets $\langle \cdots \rangle$ denote an ensemble average in an open system. $\delta_{\alpha\beta}$ is the Kronecker delta (equal to 1 when $\alpha = \beta$ and zero otherwise), and V is the volume of the subvolume. A subvolume V is characterised by its shape and linear size L. Table 1 shows the shapes considered in this work and the maximum distance between two points inside the subvolume, $L_{\max}$. As in the SSM, KB integrals for finite subvolumes, $G_{\alpha\beta}^V$, scale with the inverse of the size of the subvolume, $1/V^{1/D} \sim 1/L$, in which D is the dimensionality [14]. To find KB integrals in the thermodynamic limitm ($G_{\alpha\beta}^\infty$), extrapolation to $V \to \infty$ ($1/L \to 0$) is performed.

For convex subvolumes, Krüger and co-workers [14] have shown that the fluctuations of Equation (1) can also be expressed as integrals over the radial distribution function (RDF) $g_{\alpha\beta}(r)$,

$$G_{\alpha\beta}^V = \int_0^{L_{\max}} \mathrm{d}r \left[g_{\alpha\beta}(r) - 1\right] c(r) w(x) \qquad (2)$$
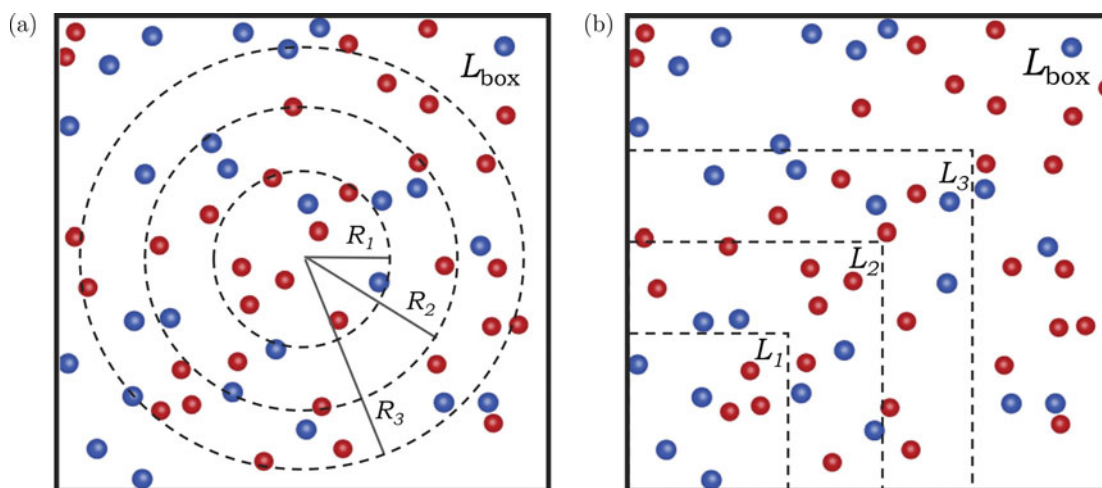
Figure 1. Computing particle fluctuations inside finite spherical (a) or cubic (b) subvolumes that are embedded inside a larger simulation box with a length L_{box} (Equation (1)). The size of the subvolume is gradually increased. For a selected molecule, one can immediately see in which subvolume the molecule is present or not.

Equation (2) is valid for subvolumes of any shape, provided the geometrical function $w(x)$ is known for that shape.

The objective of this work is to present a unified framework to compute KB integrals for subvolumes of arbitrary convex shape. We provide a numerical method to compute the function $w(x)$ based on Umbrella Sampling Monte Carlo (MC). Once the function $w(x)$ is computed for a specific shape, it can be used for any size of the subvolume. We compute the function $w(x)$ for the following shapes: square, cube, and spheroids and cuboids with different aspect ratios. Numerical tables of these functions are provided in the Supporting Information (Online). We also investigate the effect of the shape of the subvolume on the computation of KB integrals. We will show that using a cubic or spherical subvolume leads to the same KB integral in the thermodynamic limit, and that for sufficiently large subvolumes KB integrals scale as area over volume, independent of the shape of the subvolume.

The paper is organised as follows. In Section 2, the numerical method used to compute $w(x)$ is introduced. The method is verified by comparing our numerical results to the analytic expressions for a sphere (3D), circle (2D), and line (1D). In Section 3, the function $w(x)$ is computed numerically for a cube and for spheroids and cuboids with different aspect ratios. From this, finite volume KB integrals for a liquid with a model RDF are computed for various shapes, and we discuss the universality of $w(x)$ and its consequences. Our findings are summarised in Section 4.

2. Numerical computation of $w(x)$

In this section, we present a numerical method to compute the function $w(x)$ for convex subvolumes. Table 1 shows a schematic representation of the shapes studied here. For cuboids and spheroids, $w(x)$ depends on the aspect ratio a, and so $w(x)$ is computed for each a.

To find $w(x)$, we first compute $w(r) = w(x^{\star}L_{\text{max}})$ and then normalise the distance r using the maximum distance between two points in the subvolume, L_{max} (see Table 1). The function $w(r)$ is proportional to the probability distribution function $p(r)$ for finding two points inside the subvolume V, separated by distance r [14], divided by the hyperspherical volume element. Therefore, by construction we obtain $w(r = 0) = 1$ and $w(r = L_{\text{max}}) = 0$, so consequently $w(x = 0) = 1$ and $w(x = 1) = 0$. To compute the probability distribution function $p(r)$ numerically, distances between two points inside the subvolume are divided into N bins $(i_1, i_2, \ldots, i_N)$ of equal sizes, separated by Δr. Each bin contains all distances between $i\Delta r$ and $(i - 1)\Delta r$. As a result of this discretisation, we sample the probability $p(i)$, which is then used to compute $w(i)$. The value of Δr has to be chosen such that the function $p(i)$ is properly sampled. We find that a small value of Δr results in poor statistics, especially in the first few bins. We recommend setting Δr to $L/100$. To further improve the statistics, Umbrella Sampling [24,25] is implemented for computing $w(x)$. This introduces a weight function $W(i)$ which modifies the distribution of sampled distances.

2.1. Importance sampling algorithm for computing $p(i)$

In the algorithm below, we show how the probability distribution function $p(i)$ and the weight function $W(i)$ are computed. Note that the algorithm presented in this work is for a 3D subvolume; however, it is trivial to adjust it to

another dimension. The algorithm follows the following steps:

(1) Set Δr and the maximum allowed displacement for random displacements.
(2) Set a weight function $W(i)$ to zero for all bins.
(3) Choose two random points (P_1 and P_2) inside the subvolume V.
(4) For each sampling cycle (we typically performed 10^{11} cycles):
    (a) Select a point, P_1 or P_2, randomly. Assume that P_i is selected (the other point is denoted by P_j).
    (b) Add a random displacement to point P_i leading to P_{new}.
    (c) Check if this new position falls inside the subvolume. If it does not, skip to step (f), otherwise carry on with the next step.
    (d) Determine the normalised distance, r/L_{max}, between P_{new} and P_j and determine the bin number corresponding to this distance, i_{new}. The bin number corresponding to the old distance is denoted by i_{old}.
    (e) Accept or reject the displacement if a uniformly distributed random number between 0 and 1 is less than $\exp[W(i_{new}) - W(i_{old})]$. If the displacement trial move is accepted, update P_i and i_{old} such that $P_i = P_{new}$ and $i_{old} = i_{new}$.
    (f) Compute the normalised distance between P_i and P_j and the bin number, i corresponding to that distance. Update the sampling of the observed probability distribution function $p_{biased}(i)$.
(5) After a large number of cycles, remove the bias caused by the weight function:

$$p(i) = p_{biased}(i) \exp[-W(i_{old})] \qquad (3)$$

(6) Update and save $W(i)$ for the consecutive computations of $p(i)$ using an iterative updating scheme ($W(i) \to W(i) - (1/2)\ln p_{biased}(i)$), and shift $W(i)$ so that its minimum equals zero.
(7) Repeat steps 1–4 while updating $W(i)$ until a satisfactory sampling of $p(i)$ is reached. For 10^{11} cycles, running the algorithm takes approximately 150 minutes on a modern computer.

2.2. Computing w(i)

The function $w(i)$ is proportional to the distribution function $p(i)$ divided by the volume of the bin in a hypersphere with dimension D:

$$w(i) \propto \frac{p(i)}{i^D - (i - 1)^D}. \qquad (4)$$

In Equation (4), the prefactors for the bin volumes are not included yet since in the next step $w(i)$ is normalised using the value $w(0)$. Since we do not obtain statistics at $r = 0$, we interpolate to $w(0)$ using $w(1)$ and $w(2)$,

$$w(i) \to \frac{w(i)}{w(1) - \frac{(w(2) - w(1))}{2}}. \qquad (5)$$

Similarly, distances are normalised relative to L_{max}

$$x(i) = \frac{(i - \Delta r/2)}{L_{max}}. \qquad (6)$$

3. Results

3.1. The function w(x) for cube, cuboids, and spheroids

To validate our numerical method (Section 2), we compute the function $w(x)$ for subvolumes where the analytic expressions are known (line, circle, and sphere, see Table 2). In Figure 2(a), the comparison between analytic and numerical functions $w(x)$ is shown for a line, circle, and sphere. For these shapes, the numerical results reproduce the theoretical solution very well. The average absolute difference between analytic and numerical values are 9×10^{-3}, 5×10^{-3}, and 2×10^{-4} for a sphere, circle, and line, respectively. Therefore, we can conclude that the algorithm of Section 2 can be used to numerically compute the function $w(x)$ for any convex subvolume in $1D$, $2D$, or $3D$.

Next, we compute the function $w(x)$ numerically for subvolumes where analytic expressions are not available. In Figure 2(b), we show the function $w(x)$ computed numerically for a cube and sphere, which are the most commonly used shapes for subvolumes. Figure 3 shows the function $w(x)$ for spheroids (Figure 3(a)) and cuboids (Figure 3(b)) with the following aspect ratios, $a = 0.1, 1, 2, 5$, and 10. Clearly, the function $w(x)$ varies a lot with the aspect ratio a, and this function is very different for a sphere (Figure 3(a), $a = 1$) and a cube (Figure 3(b), $a = 1$). We found that it is difficult to accurately fit $w(x)$ with polynomial functions. In the Supporting Information (Online), we provide tabulated data of the function $w(x)$ for these shapes of the subvolumes. Interpolation can be used to find $w(x)$ for any value of x.
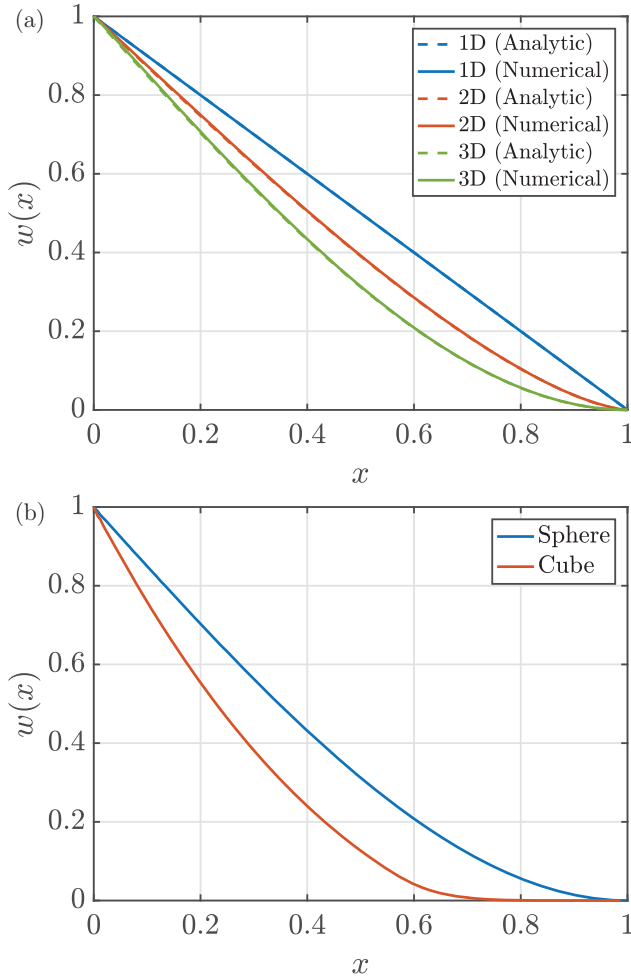
Figure 2. (Colour online) (a) The function $w(x)$ for a line (1*D*), circle (2*D*), and a sphere (3*D*). The function $w(x)$ is computed numerically using the MC algorithm provided in Section 2 and the analytic functions are listed in Table 2. In all cases, the numerical solution matches the theoretical expressions of $w(x)$. (b) The function $w(x)$ for a sphere and a cube.

3.2. KB integrals

Using the functions $w(x)$, we compute KB integrals for subvolumes with different shapes. We will focus on 3*D* systems as these are most relevant for applications. The expression for KB integrals of finite subvolumes, $G_{\alpha\beta}^{V}$, is provided by Equation (2). The distance dependent function $c(r)$ is provided in Table 2. To investigate shape effects, a liquid with the following analytic RDF model [10,26] is used:

$$g(r) - 1 = \begin{cases} \frac{3/2}{r/\sigma} \exp\left[\frac{1-r/\sigma}{\chi}\right] \cos\left[2\pi\left(\frac{r}{\sigma} - \frac{21}{20}\right)\right] & \frac{r}{\sigma} \geq \frac{19}{20}, \\ -1 & \frac{r}{\sigma} < \frac{19}{20} \end{cases}$$

$$(7)$$

where σ is the diameter of the particles, and χ is the length scale at which the fluctuations of the RDF decay. This RDF mimics density fluctuations around a central
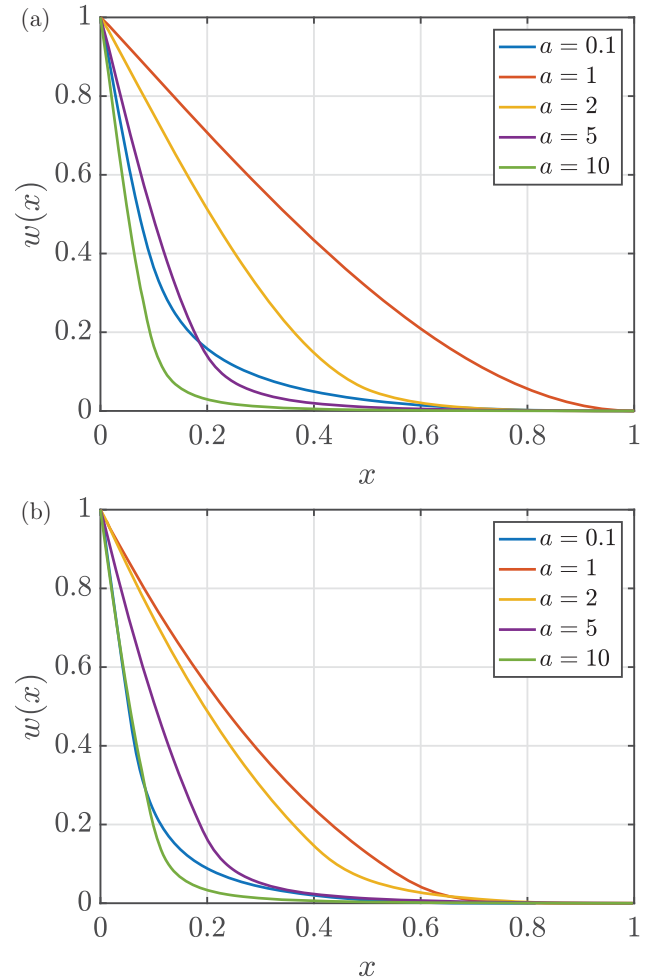

Figure 3. (Colour online) The function $w(x)$ computed numerically using the MC algorithm provided in Section 2, for (a) spheroids and (b) cuboids with different aspect ratios a.

particle for a typical isotropic liquid. The RDF parameters are fixed at $\sigma = 1$ and $\chi = 2$. Here, we work with a single-component fluid and therefore the indices α and β are dropped. The use of an analytic $g(r)$ eliminates errors due to uncertainties in RDFs obtained from molecular dynamics simulations [14,16,17]. The functions $w(x)$ are obtained numerically in tabulated form, and the value of $w(x)$ at any x is obtained by interpolation. The integral of Equation (2) is calculated using the trapezoidal rule [27].

In Figure 4, we show the KB integrals for finite subvolumes, G^{V}/σ^{3}, plotted as a function of the inverse of the length of the subvolumes, σ/L. Figure 4(a) shows the KB integrals computed for spheroids with different aspect ratios ($a = 1, 2, 5, 10$), and Figure 4(b) shows the same for cuboids. As expected, in all cases, G^{V}/σ^{3} scales linearly with σ/L for large L. In Figure 4(a), we use both analytic and numerical functions $w(x)$ for spherical subvolumes ($a = 1$). Integrating using the analytic or numerical function $w(x)$ yields practically identical values of the KB integrals, and differences are of the same order as the error
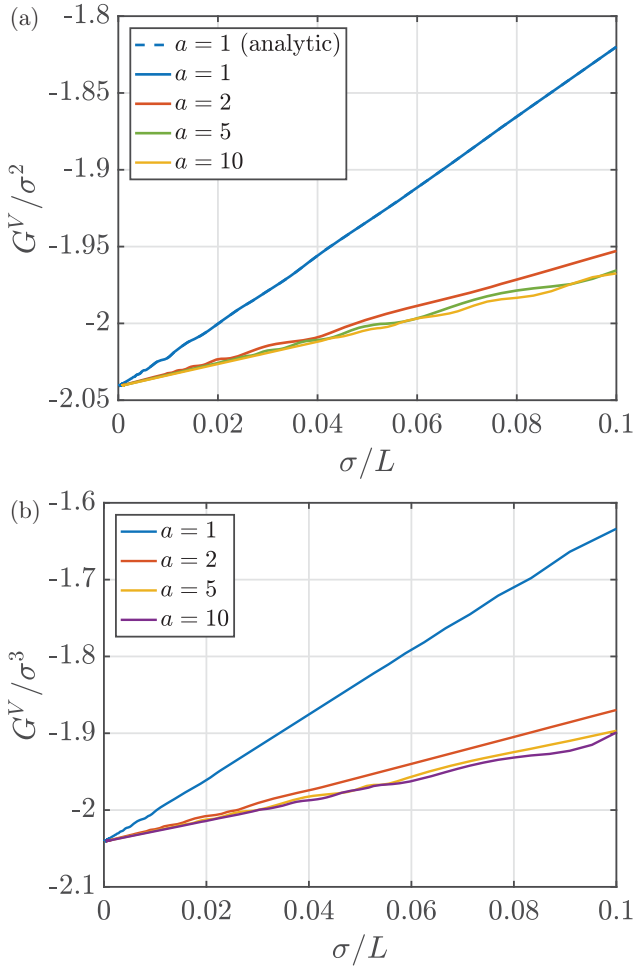
Figure 4. (Colour online) KB integrals of finite subvolumes G^V/σ^3 vs. the inverse of the size of the subvolume (σ/L) using the numerically computed $w(r)$. The subvolumes used have the following shapes: (a) spheroids and (b) cuboids with different aspect ratios a. In (a), we also compare the KB integral for a sphere ($a = 1$) using both the numerical $w(x)$ and the analytic $w(x)$ from Table 2.
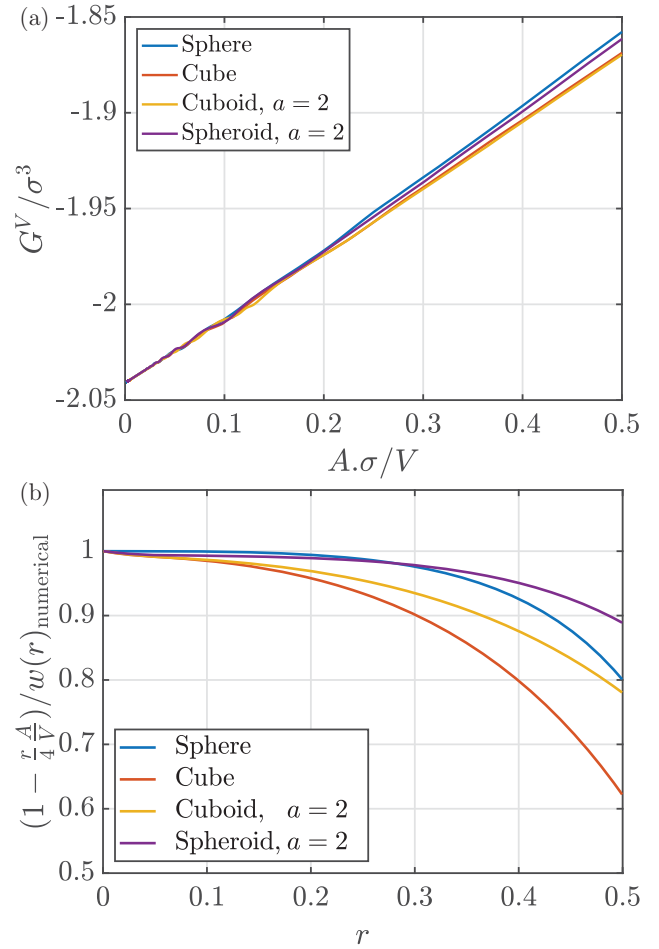

Figure 5. (Colour online) (a) KB integrals of finite subvolumes, G^V/σ^3 vs. the inverse of the surface area to volume ratio of the subvolume ($A.\sigma/V$). The KB integrals are found by numerically integrating $G^V_{\alpha\beta}$ for 3D subvolumes. (b) The ratio of $w(r)$ from Equation (8) and the numerically obtained $w(r)$.

introduced by the numerical integration of Equation (2). Changing the aspect ratio affects the slope of the lines of G^V/σ^3 versus σ/L. All lines approach the same value of the KB integral in the limit $\sigma/L \to 0$, which is expected as in the thermodynamic limit KB integrals should be independent of the shape of the subvolume. The slope dependence on the shape of the finite subvolume was previously reported in the work of Strom *et al.* [5] using arguments based on small-scale thermodynamics. These authors found that plotting KB integrals as a function of the surface-to-volume ratio of the subvolume eliminates shape effects.

In Figure 5(a), we show the KB integrals plotted as a function of the surface-area-to-volume ratio of the subvolume ($A\sigma/V$) for the following shapes: sphere, cube, spheroid with $a = 2$, and cuboid with $a = 2$. As expected from the work by Strom *et al.* [5], all KB integrals approach the same value of G^∞/σ^3 with the same slope,

and the effect of shape is only important for systems smaller than a few molecular diameters (for a sphere, $A\sigma/V > 0.5$ corresponds to $R > 6\sigma$). Close to the thermodynamic limit, G^V/σ^3 seems to be a function of $A\sigma/V$ only. For large subvolumes (and thus large L_{max}), only small values of $x = r/L_{max}$ have an important contribution $w(x)$ so one would expect that for small x, the function $w(x)$ should have a universal behaviour. Using Table 2, a Taylor expansion of $w(r)$ around $r = 0$ for a sphere yields

$$w(r) = 1 - \frac{r}{4}\frac{A}{V} + \mathcal{O}(r^2). \qquad (8)$$

In Figure 5(b), we plot the ratio of $w(r)$ from Equation (8) to the numerically computed $w(r)$, for the following shapes: sphere, cube, spheroid with $a = 2$, and cuboid with $a = 2$. A subvolume with $L = 1$ is used for all shapes. At small distances ($r < 0.1\sigma$), this ratio is practically 1 for

all shapes considered. At this range, Equation (8) provides values of $w(r)$ that are nearly identical to the numerically computed $w(r)$. This numerically confirms the universality of $w(x)$ for small x.

By neglecting the $\mathcal{O}(r^2)$ term in Equation (8) and imposing that $w(x)$ is positive, we can define a realistic model function $w(x)$ as follows:

$$w(x) = 1 - \alpha x \text{ for } x < 1/\alpha$$
$$w(x) \quad = 0 \quad \text{ for } x > 1/\alpha \qquad (9)$$

The parameter α is related to the shape of the subvolume according to Equation (8). Based on the results of the previous section, we know that elongated subvolumes will have a large value of α. By inserting Equation (9) into Equation (2) and combining with Equation (8), we obtain

$$G(A\sigma/V) = \int_0^{4V/(A\sigma)} dr 4\pi r^2 [g(r) - 1] \left[1 - \frac{rA}{4V} \right] \qquad (10)$$

which is a function of the surface area to volume ratio $A\sigma/V$, and independent of α and thus independent of the shape of the subvolume. This clearly shows that the origin of shape effects is due to the $\mathcal{O}(r^2)$ term in Equation (8), which is only important for small subvolumes.

4. Conclusions

We have introduced a method to compute KB integrals for finite subvolumes of arbitrary convex shape. This requires a numerical method to obtain the geometrical function $w(x)$, which is needed when computing KB integrals from RDFs. We showed that $w(x)$ is related to the probability of finding two particles inside a subvolume V at a certain distance, and we presented a numerical scheme based on Umbrella Sampling Monte Carlo for this. The numerical method was verified by comparing the results with analytic expressions for hyperspherical subvolumes in $1D$ (line), $2D$ (circle), and $3D$ (sphere). The method was used to compute the function $w(x)$ for subvolumes where analytic expressions are not available: square, cube, and spheroids and cuboids with different aspect ratios. These functions are tabulated in the Supporting Information (Online). We computed KB integrals for subvolumes with different shapes, using an analytic RDF model representing an isotropic liquid. In the thermodynamic limit, KB integrals are independent of the shape of the subvolume, and the approach to the thermodynamic limit only depends on the area over volume ratio, and not the shape of the subvolume. This is due

to the observation that for small r, $w(r)$ is only a function of r and the surface-to-volume ratio of the subvolume, and independent of the shape of the subvolume. One may consider the universality of $w(r)$ as a 'shape thermodynamic limit'. The difference with the conventional thermodynamic limit is that only system size dependencies are important, and not the shape. From our calculations, it seems that shape effects are only important for systems smaller than a few molecular diameters. It would be interesting to investigate whether or not these findings are applicable to molecular liquids and non-isotropic liquids.

Disclosure statement

No potential conflict of interest was reported by the authors.

ORCID

Noura Dawass ⓘ http://orcid.org/0000-0001-5234-7127
Peter Krüger ⓘ http://orcid.org/0000-0002-1247-9886
Jean-Marc Simon ⓘ http://orcid.org/0000-0002-1340-5408
Thijs J. H. Vlugt ⓘ http://orcid.org/0000-0003-3059-8712

References

[1] S.K. Schnell, X. Liu, J.M. Simon, A. Bardow, D. Bedeaux, T.J.H. Vlugt, and S. Kjelstrup, J. Phys. Chem. B **115**(37), 10911–10918 (2011). doi:10.1021/jp204347p
[2] S.K. Schnell, T.J.H. Vlugt, J.M. Simon, D. Bedeaux, and S. Kjelstrup, Chem. Phys. Lett. **504**, 199–201 (2011). doi:10.1016/j.cplett.2011.01.080
[3] S.K. Schnell, T.J.H. Vlugt, J.M. Simon, D. Bedeaux, and S. Kjelstrup, Mol. Phys. **110**, 1069–1079 (2012). doi:10.1080/00268976.2011.637524
[4] N. Dawass, P. Krüger, S.K. Schnell, D. Bedeaux, S. Kjelstrup, J.M. Simon, and T.J.H. Vlugt, Mol. Simul. in press. doi:10.1080/08927022.2017.1416114.
[5] B.A. Strøm, J.M. Simon, S.K. Schnell, S. Kjelstrup, J. He, and D. Bedeaux, Phys. Chem. Chem. Phys. **19**, 9016–9027 (2017).

[6] X. Liu, S.K. Schnell, J.M. Simon, P. Krüger, D. Bedeaux, S. Kjelstrup, A. Bardow, and T.J.H. Vlugt, Int. J. Thermophys. **34**(7), 1169–1196 (2013). doi:10.1007/s10765-013-1482-3

[7] E. Matteoli and L. Lepori, J. Chem. Phys. **80**(6), 2856–2863 (1984). doi:10.1063/1.447034

[8] S.K. Schnell, R. Skorpa, D. Bedeaux, S. Kjelstrup, T.J.H. Vlugt, and J.M. Simon, J. Chem. Phys. **141**(14), 144501 (2014). doi:10.1063/1.4896939

[9] J.G. Kirkwood and F.P. Buff, J. Chem. Phys. **19**(6), 774–777 (1951). doi:10.1063/1.1748352

[10] J.G. Kirkwood and E.M. Boggs, J. Chem. Phys. **10**(6), 394–402 (1942). doi:10.1063/1.1723737

[11] A. Ben-Naim, *Molecular Theory of Solutions* (Oxford University Press, Oxford, 2006).

[12] A. Ben-Naim, J. Chem. Phys. **67**(11), 4884–4890 (1977). doi:10.1063/1.434669

[13] D.G. Hall, Trans. Faraday Soc. **67**, 2516–2524 (1970).

[14] P. Krüger, S.K. Schnell, D. Bedeaux, S. Kjelstrup, T.J.H. Vlugt, and J.M. Simon, J. Phys. Chem. Lett. **4**(2), 235–238 (2013).

[15] X. Liu, A. MartÃn-Calvo, E. McGarrity, S.K. Schnell, S. Calero, J.M. Simon, D. Bedeaux, S. Kjelstrup, A. Bardow, and T.J.H. Vlugt, Ind. Eng. Chem. Res. **51**(30), 10247–10258 (2012). doi:10.1021/ie301009v

[16] J. Milzetti, D. Nayar and N.F.A. van der Vegt, J. Phys. Chem. B. in press. doi:10.1021/acs.jpcb.7b11831.

[17] P. Ganguly and N.F.A. van der Vegt, J. Chem. Theory Comput. **9**(3), 1347–1355 (2013). doi:10.1021/ct301017q

[18] P.E. Smith, E. Matteoli, and J.P. O'Connell, *Fluctuation Theory of Solutions: Applications in Chemistry, Chemical Engineering, and Biophysics* (CRC Press, Boca Raton, FL, 2013). doi:10.1201/b14014

[19] A. Ben-Naim, J. Chem. Phys. **138**(22), 224906 (2013). doi:10.1063/1.4810806

[20] V. Pierce, M. Kang, M. Aburi, S. Weerasinghe, and P.E. Smith, Cell Biochem. Biophys. **50**(1), 1–22 (2008). doi:10.1007/s12013-007-9005-0

[21] G. Giambasu, T. Luchko, D. Herschlag, D. York, and D. Case, Biophys. J. **106**(4), 883–894 (2014). doi:10.1016/j.bpj.2014.01.021

[22] R. Cortes-Huerto, K. Kremer, and R. Potestio, J. Chem. Phys. **145**(14), 141103 (2016). doi:10.1063/1.4964779

[23] M.M. Reif, M. Winger, and C. Oostenbrink, J. Chem. Theory Comput. **9**(2), 1247–1264 (2013). doi:10.1021/ct300874c

[24] G. Torrie and J. Valleau, J. Comput. Phys. **23**(2), 187–199 (1977). doi:10.1016/0021-9991(77)90121-8

[25] D. Frenkel and B. Smit, *Understanding Molecular Simulation: From Algorithms to Applications*, 1 vols. (Academic Press, Cambridge, MA, 2001).

[26] L. Verlet, Phys. Rev. **165**(1), 201–214 (1968). doi:10.1103/PhysRev.165.201

[27] D.V. Griffiths and I.M. Smith, *Numerical Methods for Engineers* (CRC Press, Boca Raton, FL, 2006).